Reactions of Cobalt Cluster Anions with Oxygen, Nitrogen, and Carbon Monoxide

Elizabeth Kapiloff and Kent M. Ervin*

Department of Chemistry and Chemical Physics Program, University of Nevada, Reno, Nevada 89557

Received: July 24, 1997; In Final Form: September 8, 1997[⊗]

The chemical reactivity of cobalt cluster anions, Co_n^- ($n = 2-8$), toward O_2, N_2, and CO is investigated by flow tube reactor kinetics. The reactivity is highest for the reactions with O_2 and intermediate for CO, while the clusters are nearly inert toward N_2. Only the largest clusters studied, Co_7^- and Co_8^-, show any evidence for reaction with nitrogen by addition of N_2 at very slow rates. Reactions with O_2 have rapid rate coefficients that are largely independent of cluster size and lead to extensive fragmentation of the clusters. The rate coefficients with CO increase with increasing cluster size. Sequential addition of CO to the cobalt cluster anions leads to the saturated species: $Co_2(CO)_7^-$, $Co_3(CO)_{10}^-$, $Co_4(CO)_{12}^-$, $Co_5(CO)_{13}^-$, and $Co_6(CO)_{15}^-$. Skeletal structures are proposed for these saturated clusters in accordance with electron-counting rules.

1. Introduction

Transition metal clusters exhibit a wide variety of reactive behavior, often exhibiting greatly different reactivities for different sizes, charge states, and neighboring elements.[1,2] Studying the cluster size- and charge-dependence of the reactivity provides insight into the relationships between electronic or geometric structure and the chemical reactivity. Characterizing the interactions of transition metal clusters with simple adsorbate molecules is an initial step in elucidating their potential as models of catalytic processes. Cobalt clusters have been studied in part because of cobalt's importance as a catalytic metal, in Fischer−Tropsch synthesis of hydrocarbons from CO and H_2, for example.[3,4]

Reactivity studies have been reported for neutral and cationic cobalt clusters. Neutral[5−11] and cationic[12] cobalt clusters react with hydrogen by dissociative chemisorption with strongly size-selective rates. Reactions of the neutral[6,13] and cationic[14] clusters with carbon monoxide, in contrast, proceed by molecular addition and exhibit little size selectivity but instead have gradually increasing rate coefficients with cluster size. Both neutral[6,15−17] and cationic[12,15] cobalt clusters are observed to react with N_2 with strong size-selectivity. Cobalt clusters tend to be very reactive with oxygen, with both cations[18−20] and neutrals[11] forming cobalt oxides, often with loss of cobalt atoms from the cluster. Reactions of cobalt clusters with hydrocarbons have also been observed.[12,21−25]

Riley and co-workers[10,16,17,26−32] have utilized chemisorption reactions with nitrogen, water, ammonia, and hydrogen as chemical probes of the structure of bare and hydrogenated neutral cobalt clusters. These experiments give evidence for icosahedral packing for large clusters Co_n ($n > 50$), with other structures for small clusters. Intensity distributions in cobalt cluster mass spectra[33] tend to agree with icosahedral shell structure. Other physical properties known for cobalt clusters include binding energies of Co_n^+ measured by collision-induced dissociation[19,34] or photodissociation,[35,36] ionization potentials measured by photoionization,[37,38] photoabsorption spectra,[39] and electron affinities measured by negative ion photoelectron spectroscopy.[40,41] Few theoretical studies of cobalt cluster structures have been carried out.[42,43] Recent density functional calculations[43] indicate the neutral trimer is triangular and that the tetramer is a distorted tetrahedron. These structures agree with those inferred from photodissociation spectroscopy[39] of Co_nAr^+.

Studying the size-selected reactivities of different cluster charge states yields information that can help differentiate between geometric and electronic effects in these clusters. To our knowledge, no previous reaction studies have been conducted on anionic cobalt clusters larger than dimers. The reactivity of cobalt cluster anions Co_n^- ($n = 2-8$), with three reactant gases O_2, N_2, and CO are examined in this work and compared with the previous studies on cationic and neutral cobalt clusters with these reagents. Skeletal structures of the clusters saturated with carbonyls are predicted using electron-counting rules,[44−50] which previously have been applied to cationic cobalt cluster carbonyls[14,21,22] and nickel group cluster carbonyls.[51−54]

2. Experimental Methods

A flow tube reactor (flowing afterglow) apparatus is used to measure reaction rates and product distributions. Details of the instrument and data analysis procedures have been presented previously.[53,54] Cobalt cluster anions are produced in the flow tube using a dc discharge sputtering source with cobalt foil (99.99%, Aldrich) covering the cathode. Clusters are sputtered from the cathode and swept downstream by the buffer gas, which consists of helium (Sierra Gas, 99.995%) with up to 5% argon (Spectra Gases, 99.999%) at a total pressure of 0.4−0.6 Torr (50−80 Pa). The pressure and flow rates are chosen to provide a viscous laminar flow in the 7.3 cm diameter flow tube. The ions drift at least 80 cm down the flow tube and undergo 10^4-10^5 collisions before reaching the reaction zone. These thermalizing collisions are intended to quench the initial vibrational and electronic excitation of the parent clusters.

Reactant gases are introduced through a ring inlet, which can be moved to change the reaction zone length. Reactant gases are O_2 (Sierra Gas), N_2 (Sierra Gas), and CO (Matheson) of >99.99% purity used without further purification. At the end of the flow tube, the reactant and product ions are sampled through a 1 mm diameter aperture in a nose cone and are subsequently analyzed by a quadrupole mass spectrometer. To obtain absolute thermal rates, the reactant ion intensities are measured as a function of reagent flow rate at a fixed reaction zone length under pseudo-first-order conditions. We report effective bimolecular rate coefficients at the buffer gas pressure.

* To whom correspondence should be addressed. E-mail: ervin@chem.unr.edu.

[⊗] Abstract published in *Advance ACS Abstracts,* October 15, 1997.

S1089-5639(97)02404-3 CCC: $14.00

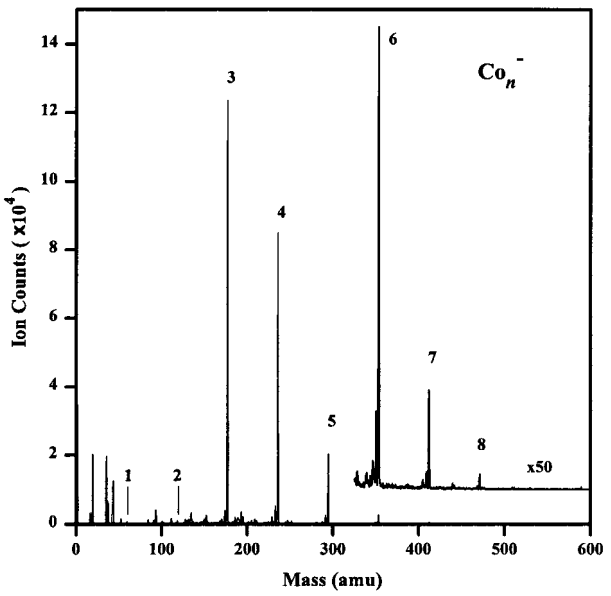

Figure 1. Mass spectrum of cobalt cluster anions from flow tube reactor source. Peaks corresponding to bare Co_n^- clusters are labeled by *n*. Other peaks are impurity ions.

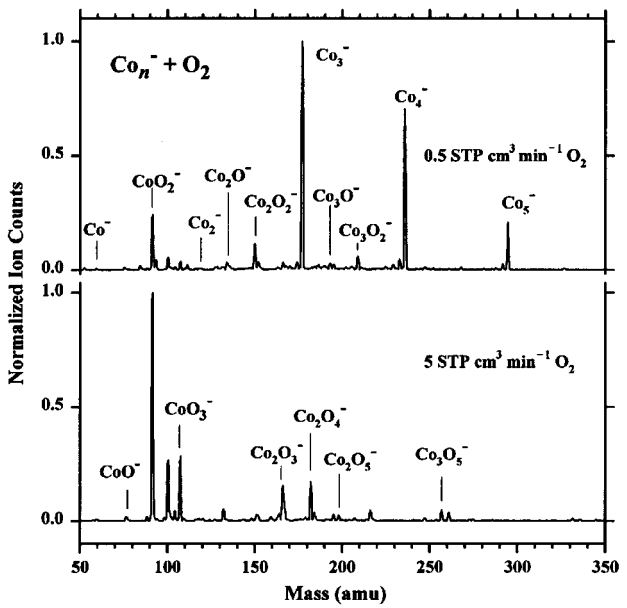

Figure 2. Mass spectra with addition of 0.5 STP cm^3 min^{-1} (top) and 5.0 STP cm^3 min^{-1} (bottom) flow rate of oxygen in flow tube. Major cobalt oxide anion products are labeled.

Several scans obtained under different conditions and at different times are averaged to determine the overall rate of reaction. Reported uncertainties are the 95% confidence interval of the mean. The estimated absolute uncertainty of the measured rate coefficients is about ±30%, based on calibrations with known reactions.[53,54]

Because the initial clusters are not mass selected before reaction in these experiments, it is not always possible to determine the detailed product channel branching ratios for a given cluster size, especially when metal−metal bond-breaking channels are significant. Nevertheless, general trends can be followed by taking scans of the ionic products as a function of reagent concentration in the flow tube, and the most stable product species can be identified.

3. Results

A mass spectrum of the parent cobalt cluster anions without the addition of any reactant gas is shown in Figure 1. Cobalt clusters Co_n^- with sizes up to $n = 8$ are observed with intensities sufficient for kinetics measurements. The highest-intensity peak in the spectrum is Co_3^-, with decreasing intensities for larger sizes. Atomic and diatomic cobalt anions are present at low intensities. Various impurity anions are also present. These arise from surface contamination on the cobalt cathode or from reactions with gas-phase impurities. Because cobalt has a single isotopic mass, the impurities can be readily distinguished from pure clusters.

3.1. Oxygen Reactions. When O_2 is administered as the reactant gas, the mass spectrum changes radically, as shown in Figure 2, which compares mass spectra with a small amount and a large amount of oxygen added. Upon the introduction of O_2 gas at the higher flow rate the parent clusters have disappeared and the peaks have shifted to lower masses. The most intense peak at high O_2 flow rates is CoO_2^-. Other cobalt oxide anions present to appreciable extent are those containing one or two cobalt atoms, while oxides with up to four cobalt atoms are 1−2 orders of magnitude lower in intensity. This behavior indicates that the primary processes are those in which oxidation occurs by removal of one or two metal atoms from the cluster to form the small metal oxide anion, leaving the rest of the cobalt cluster behind as neutral products.

The measured effective bimolecular reaction rate coefficients for $Co_n^- + O_2$ ($n = 2-7$) are presented in Table 1 and Figure 3 and are compared with the calculated Langevin collision rates. The reaction efficiencies relative to the collision rate are high, 31%−54% for sizes $n = 2-7$. There is little dependence of the reaction efficiency on the cobalt cluster size, which implies that the oxidation reactions are driven by their exothermicity and are not sensitive to the structure of the clusters.

Figure 4 shows representative plots of $Co_nO_m^-$ product ion intensities as a function of oxygen flow rate for $n = 1-5$. The presence of $Co_nO_m^-$ ions at zero O_2 reactant gas flow is due to oxide impurities from the ion source. Both bare Co_n^- clusters and Co_nO^- monoxides react rapidly upon addition of O_2. Higher oxides, $Co_nO_m^-$ ($n \geq 2$ and $m = 2-4$), show initial increases, indicating they are product species, but these also react at higher O_2 concentrations. CoO^-, CoO_2^-, CoO_3^-, and $Co_2O_3^-$ products show an initial rise and then a plateau, indicating that these ions are relatively stable with respect to further oxidation. The relative intensities of products at high oxygen concentrations (Figure 2) give an indication of the overall stability of the oxide species. The trend in stability is roughly $CoO_2^- > CoO_3^- > (Co_2O_3^-, Co_2O_4^-) > (Co_3O_5^-, Co_2O_5^-, CoO^-)$.

The sum of the intensities of the CoO_m^- and $Co_2O_m^-$ products for all *m* surpasses the initial intensities of Co^- and Co_2^-, respectively, which indicates the products arise largely from reactions of larger clusters. The sums of the intensities of $Co_3O_m^-$, $Co_4O_m^-$, and $Co_5O_m^-$ species over *m* decline with increasing flow rate, which shows that most of the Co_n^- and Co_nO^- ($n \geq 3$) clusters lose metal atoms upon oxidation, or are lost by reactive electron detachment. Over 99% of the initial intensities for Co_3^-, Co_4^-, and Co_5^- and over 95% for Co_6^- and Co_7^- are depleted by O_2 flow rates of 150 cm^3 min^{-1} at standard temperature and pressure (STP).

3.2. Carbon Monoxide Reactions. The total effective bimolecular rate coefficients for reaction of Co_n^- ($n = 3-8$) with CO, shown in Figure 3 and Table 1, monotonically increase with cobalt cluster size from Co_3^-, which reacts in 6% of the collisions, to Co_8^-, which reacts at nearly 50% of the collision rate. The observed initial products are Co_nCO^- species, formed either by simple addition of CO or by addition combined with

TABLE 1: Rate Coefficients (10^{-10} cm^3 s^{-1}) for Reactions of Cobalt Cluster Anions with O_2, CO, and N_2

Co_n^-	oxygen			carbon monoxide			nitrogen		
n	k_{exp}[a]	k_c[b]	k_{exp}/k_c	k_{exp}[a]	k_c[b]	k_{exp}/k_c	k_{exp}[a]	k_c[b]	k_{exp}/k_c
2	2.9 ± 1.0	5.9	0.49				<0.01	6.5	<0.002
3	2.5 ± 0.6	5.7	0.44	0.4 ± 0.2	6.7	0.06	<0.01	6.3	<0.002
4	1.7 ± 0.4	5.5	0.31	0.59 ± 0.17	6.5	0.09	<0.01	6.2	<0.002
5	2.0 ± 0.5	5.5	0.36	1.3 ± 0.4	6.5	0.20	<0.01	6.1	<0.002
6	2.2 ± 0.8	5.4	0.40	1.8 ± 0.6	6.4	0.28	<0.01	6.1	<0.002
7	2.9 ±0.8	5.4	0.54	2.2 ± 0.7	6.4	0.34	<0.01	6.0	<0.002
8				3.0 ± 1.0	6.4	0.47			

[a] Measured effective bimolecular rate coefficient. [b] Calculated collision rate.

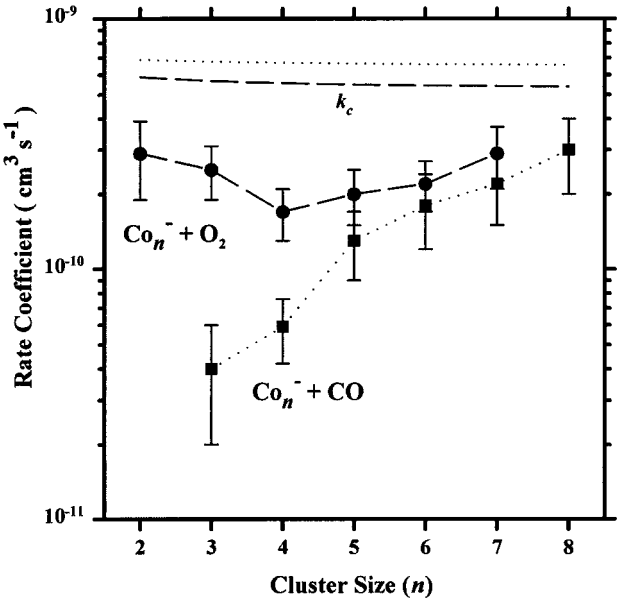

Figure 3. Effective bimolecular rate coefficients for reaction of cobalt cluster anions with O_2 (circles and broken line) and CO (squares and dotted line). The lines labeled k_c are the calculated collision rates.

loss of cobalt atom(s) from the cluster. Sequential addition of carbonyls is observed at higher CO concentrations.

The mass spectrum shown in Figure 5 was taken at a very high CO flow rate, at approximately $p_{CO} = 0.05$ Torr or 10 mole % CO in He, at which most of the parent clusters have been saturated with CO. The clusters $Co_2(CO)_7^-$, $Co_3(CO)_{10}^-$, $Co_4(CO)_{12}^-$, $Co_5(CO)_{13}^-$, and Co6$(CO)_{15}^-$ are assigned as the saturation limits because they have the most carbonyls observed for each cobalt cluster size under the accessible range of conditions. Saturation limits are discussed further below. The other peaks in Figure 5 represent clusters with intermediate degrees of saturation or impurities, which are mostly cobalt oxides with varying numbers of carbonyls attached.

Representative cobalt carbonyl product scans are shown in Figure 6 for $Co_n(CO)_m^-$ ($n = 3-6$, $m = 0-15$). The general trend is that the bare clusters react with rapid sequential addition of multiple carbonyls. However, the rates of sequential additions are not always uniform up to the saturation limit. For example, the $n = 5$ plot shows rapid addition of carbonyls to Co_5^- up to $Co_5(CO)_9^-$, which is the major species by a CO flow rate of 2 STP cm^3 min^{-1}. Additions of the 10th through 13th carbonyl then occur at a significantly slower rate, with the $Co_5(CO)_{13}^-$ species becoming the most abundant above 12 STP cm^3 min^{-1}. Above 30 STP cm^3 min^{-1}, the intensities of $Co_5(CO)_9^-$ and $Co_5(CO)_{13}^-$ are constant with further increases in CO flow rate, indicating a quasi-equilibrium distribution with the latter species favored by a factor of 8. Thus, although we identify $Co_5(CO)_{13}^-$ as the "saturated" pentacobalt carbonyl cluster, $Co_5(CO)_9^-$ is also a relatively stable species.

Some other cluster sizes also show evidence of an intermediate "bottleneck" in the sequential addition kinetics followed by further addition up to a saturation limit. Table 2 summarizes both the saturated species and the intermediate stable ions. The stable dicobalt carbonyls, $Co_2(CO)_6^-$ and $Co_2(CO)_7^-$, have intensities higher than the initial Co_2^- intensity and therefore must arise from larger clusters via cobalt atom loss upon reaction with CO. For $n = 3$, the sequential addition occurs relatively slowly, consistent with Co_3^- having the slowest total rate coefficient for $n \geq 3$. $Co_3(CO)_8^-$ is the predominant species above 5 STP cm^3 min^{-1}, but $Co_3(CO)_9^-$ and $Co_3(CO)_{10}^-$ are still rising up to the highest accessible flow rates while $Co_3(CO)_8^-$ declines slowly. There is no evidence for formation of $Co_3(CO)_{11}^-$, however, so $Co_3(CO)_{10}^-$ is assigned as the saturation limit. For $n = 4$, sequential addition is fairly rapid up to $Co_4(CO)_{11}^-$ (with a slight bottleneck at $Co_4(CO)_9^-$). $Co_4(CO)_{11}^-$ is the dominant species above a CO flow rate of 7 STP cm^3 min^{-1}, but $Co_4(CO)_{12}^-$ is being formed very slowly at high flow rates. Since there is no evidence of $Co_4(CO)_{13}^-$ formation, we assign $Co_4(CO)_{12}^-$ as the saturated species. For $n = 6$, rapid addition of carbonyls occurs up to $Co_6(CO)_{12}^-$, which becomes most abundant above 2.5 STP cm^3 min^{-1}. Slower additions occur sequentially up to $Co_6(CO)_{15}^-$, which is the most abundant above 45 STP cm^3 min^{-1} and is the only hexacobalt species present at the highest flow rates. For $n = 7$ (not shown), sequential addition is also observed, but because of small initial intensities, the kinetics is difficult to follow. The largest heptacobalt carbonyls species observed in the mass spectra is $Co_7(CO)_{16}^-$ at high CO flow rates, but this species is still increasing at the highest CO concentrations in the product kinetics scans. It is likely that for these and larger clusters, the number carbonyls added is limited by the reaction time in the flow tube (about 5 ms) rather than by intrinsic saturation.

The flow scans in Figure 6 show that fragmentation processes occur in addition to sequential addition of carbonyls. At the highest CO flow rate of 150 cm^3 min^{-1}, the sum of $Co_n(CO)_m^-$ intensities for all m represent 60% of the initial Co_n^- parent cluster intensity for $n = 3$, 17% for $n = 4$, and less than 10% for $n = 5$ and $n = 6$. Some of the fragmentation likely proceeds by loss of cobalt atoms or cobalt cluster fragments upon reaction of larger clusters with CO. Most of the fragmentation occurs upon the initial interactions with CO. Once a few carbonyls have been adsorbed, those clusters tend to continue to add CO without further fragmentation, as shown in Figure 6 by comparing the intensities of highly ligated species at high CO concentrations to the maximum intensities of clusters with one to three carbonyls.

Additional evidence of fragmentation processes is provided by nonlinear decays of some clusters at intermediate flow rates, for example, for $n = 3$ clusters in the vicinity of 3 STP cm^3 min$^-$,[1] which indicates that they are also produced from reactions of larger clusters. The total $Co_n(CO)_m^-$ intensity at the highest flow rates is less than the sum of all Co_n^- parent intensities. That implies that reactive electron detachment

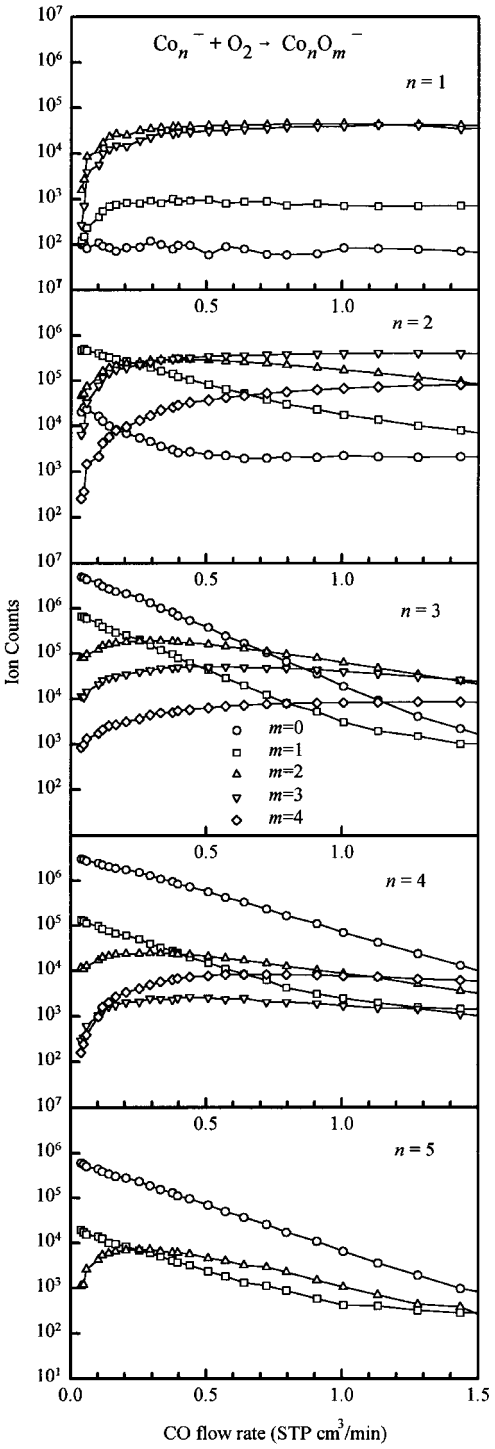

Figure 4. Product ion intensities from the reaction of Co_n^- with oxygen as a function of O_2 flow rate. $Co_nO_m^-$ ions are grouped by n from $n = 1$ to $n = 5$ (top to bottom panels), and m values are given by the symbols according to the legend in the center panel. Some $Co_nO_m^-$ ions are initially present at zero O_2 flow rate owing to impurities from the metal cathode discharge ion source.

reaction channels, for which the neutral products cannot be observed directly, are significant. However, some of the decrease in total ion intensity could be due to changes in ion source characteristics or ion sampling efficiency at high CO concentrations.

3.3. Nitrogen Reactions. The reactions of cobalt cluster anions with N_2 gas are extremely slow. The mass spectrum of the cobalt clusters remains qualitatively unchanged with nitrogen gas addition as high as 0.02 Torr (3 Pa) in the flow tube, about 4 mole % in the helium/argon buffer gas. Based on the flat

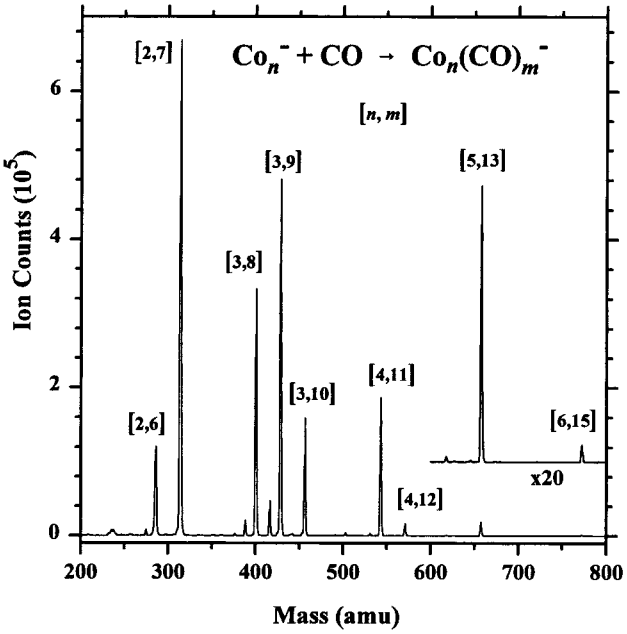

Figure 5. Mass spectrum at high CO flow rates corresponding to $p_{CO} = 0.05$ Torr. $Co_n(CO)_m^-$ ions are identified by $[n,m]$. Small peaks are cobalt oxides ions with added carbonyls or other impurities.

cluster ion intensities as a function of nitrogen concentration, the rate coefficients are at least 3 orders of magnitude slower than the Langevin collision rate below the experimental limit for reliable measurements. The upper limit rate coefficients are $k < 10^{-12}$ cm^3 s^{-1} for $Co_n^- + N_2$ ($n = 2-7$).

No products were observed for Co_n^- ($n \leq 6$), but the Co_7^- cluster shows a significant decay and formation of the addition product $Co_7(N_2)^-$, as shown in Figure 7. The N_2 flow rates at which $Co_7(N_2)^-$ is observed are high, greater than we consider acceptable for quantitative measurement of reaction rates because of possible changes in flow and ion sampling characteristics in the flow tube. Mass spectra show evidence of product formation from the octamer, $Co_8(N_2)^-$, but the Co_8^- ion intensity was too low to obtain flow scan data. $Co_7(N_2)^-$ and $Co_8(N_2)^-$ are the only products whose intensity increase is definitely significant compared with the intensities of impurities. Reactions from residual CO (also 28 amu) in the gas handling system were observed in preliminary experiments. These reactions were avoided by carrying out the nitrogen reactions with a freshly cleaned system. Carbon monoxide cannot be responsible for the observed $Co_7(N_2)^-$ product because smaller Co_n^- ($n \leq 6$) clusters would also have reacted in the presence of CO.

4. Discussion

4.1. Reactivity and Thermochemical Trends. The major trends in reactivity for O_2, CO, and N_2 with cobalt cluster anions may be summarized as follows. (1) Oxygen reacts with all cluster sizes indiscriminately and with extensive breaking of metal and oxygen bonds. (2) Carbon monoxide adds to the clusters with no evidence of breaking CO bonds and with much less fragmentation of the metal cores. The total reaction rate coefficients increase monotonically with cluster size. Sequential addition of carbonyls occurs up to size-specific saturation limits, with evidence for intermediate stable species. (3) The cobalt clusters are nearly inert toward N_2, but the largest sizes studied ($n = 7-8$) exhibit slow addition of a single nitrogen molecule.

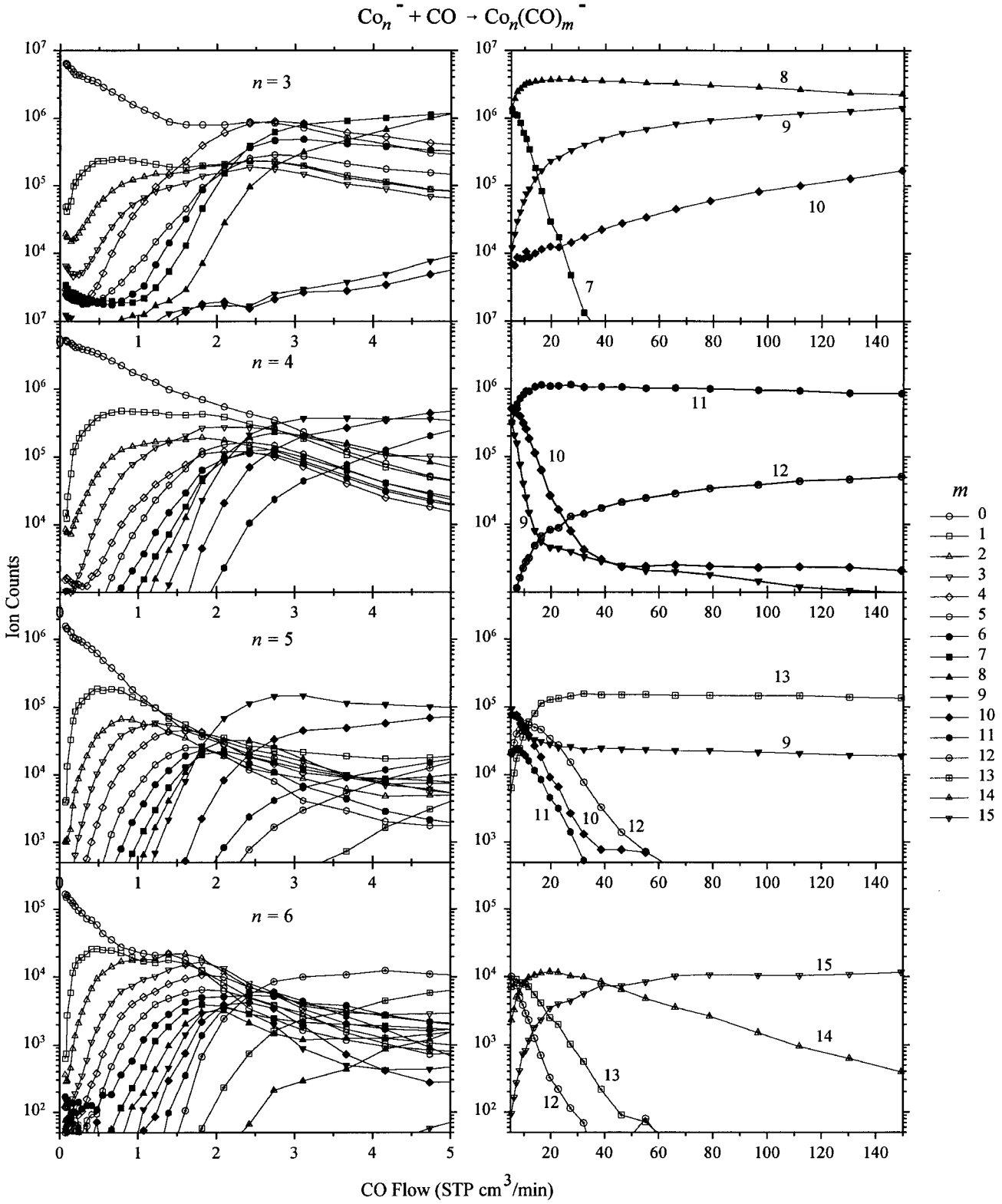

Figure 6. Product ion intensities from the reaction of Co_n^- with carbon monoxide as a function of CO flow rate. $Co_n(CO)_m^-$ ions are grouped by n from $n = 3$ to $n = 6$ (top to bottom panels), and m values are given by the symbols according to the legend at the right. The left panels show all products at low CO flow rates (0−5 STP cm^3 min^{-1}), while the right panels show only the species corresponding to the last few carbonyls added up to the saturation limit (labeled by m values) at higher CO flow rates.

The differences in reactivity of the three reagents can be partially explained by the relative energetics of metal−metal bond breaking and molecular or dissociative chemisorption. Dissociation energies for cobalt cluster anions have not been measured directly but can be estimated from the dissociation energies of the cationic clusters,[34] ionization potentials,[37,38] and electron affinities.[40,41] The dissociation energies are shown in Figure 8 for the cationic, neutral, and anionic cobalt clusters. The bond energies for a given cluster size for $n > 3$ are very similar for all three charge states, consistent with similar geometries and with the addition of electrons to nonbonding d orbitals from cation to neutral[34] and from neutral to anion. The nonmonotonic changes with size suggest that the clusters have a most stable ground state with definite geometry,[34] although

TABLE 2: Saturation Limits for the Cationic and Anionic Cobalt Carbonyl Clusters and Proposed Geometrical Structures

	$Co_n(CO)_m^-$ (this work)						$Co_n(CO)_m^+$ (Castleman and co-workers[14])				
	saturation limit[a]			other stable species[b]			saturation limit			other stable species[b]	
n	*m*	CVEs[c]	structure[d]	*m*	CVEs[c]	structure[d]	*m*	CVEs[c]	structure[d]	*m*	CVEs[c]
2	7	33	linear	6	31		8	33	linear		
3	10	48	triangle	8	44		10	46	"imperfect triangle"		
4	12	61	butterfly	11	59	tetrahedron	12	59	tetrahedron	6	47
5	13	72	trigonal bipyramid	9	64		14	72	trigonal bipyramid	8, 9	60, 62
6	15	85	octahedron[e]	12	79		16	85	octahedron[e]	12	77
7				16	96	tricapped tetrahedron or bicapped trigonal bipyramid	19	100	pentagonal bipyramid	14	90

[a] Species with maximum number of carbonyls coordinating to $Co_n^{\pm}$. [b] Species with less than the saturation limit of carbonyls that show relatively high kinetic stability; "magic numbers".[14] [c] Cluster valence electron count. [d] Structure predicted by polyhedral skeletal electron pair theory for given *n* and CVE count. [e] See text.

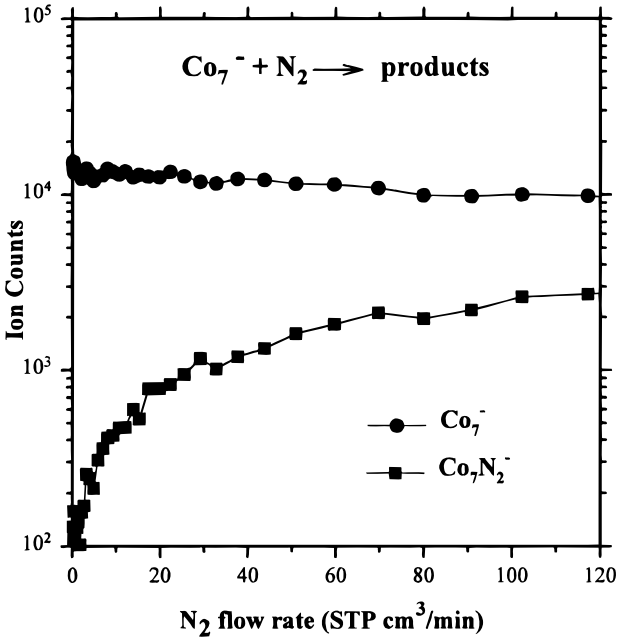

Figure 7. Ion intensities for the reaction $Co_7^- + N_2 \rightarrow Co_7(N_2)^-$ as a function of nitrogen flow rate in the flow tube reactor.

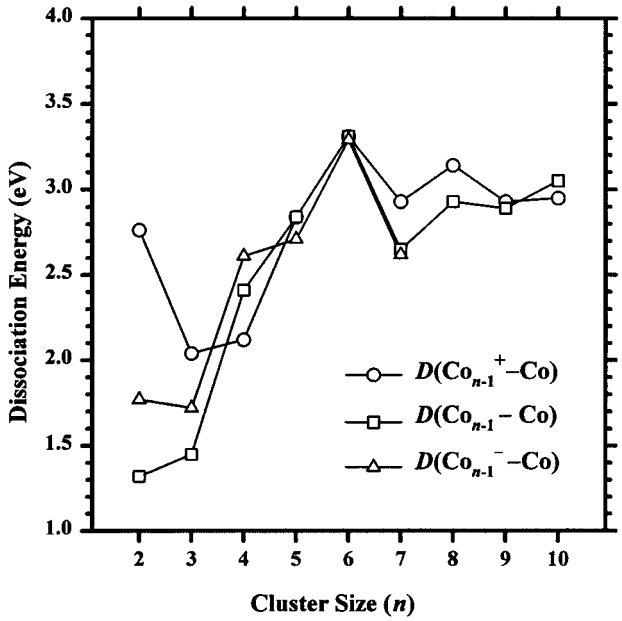

Figure 8. Cobalt cluster bond energies derived from the literature. Values for cationic clusters were measured by collision-induced dissociation experiments.[34] Values for the neutral clusters are derived using cluster ionization potentials,[34,37,38] and those for the anionic clusters are derived using electron affinities from photoelectron spectroscopy.[40,41]

isomers cannot be ruled out. Because the dissociation energies are similar for all three charge states, the reactivity differences among the charge states must be attributed to properties other than differences in metal−metal bond energies.

Adsorption energies for O_2, CO, and N_2 on cobalt clusters are not known, but rough estimates can be made based on adsorption energies for cobalt surfaces. Dissociative adsorption of oxygen on cobalt is strongly exothermic,[55] with an enthalpy of adsorption of 478 kJ/mol. Carbon monoxide adsorbs molecularly on cobalt, with an adsorption enthalpy of 100−145 kJ/mol depending on the surface.[56−58] The adsorption of nitrogen on cobalt surfaces is not known, but is expected[56,59] to be molecular, and the adsorption energy may be estimated to be no more than 20−50 kJ/mol, the values for molecular adsorption on nickel and iron.[60] The adsorption energies represent roughly the energy available to break metal−metal bonds upon reaction with the cluster. The highly exothermic adsorption of oxygen leads to dissociation of O_2 and the observed massive fragmentation of the cobalt clusters. The small adsorption energies for CO and N_2 provide smaller amounts of energy in the nascent cluster, which can be partially (CO) or completely (N_2) removed by buffer gas collisions before fragmentation occurs.

4.2. Oxygen Reactions. The high reaction efficiencies observed for the cobalt cluster anion reactions with oxygen indicate there is at most a small activation barrier for adsorption, <4 kJ/mol for Co_n^- ($n = 2-7$) based on a simple Arrhenius model. Castleman and co-workers[20] investigated the kinetics of mass-selected Co_n^+ ($n = 2-9$) clusters reacting with O_2 gas in a SIDT-LV (selected ion drift tube with laser vaporization source) for which the reaction conditions are similar to ours. They found fast oxidation reactions for all of the clusters with little variation in rates, similar to the present results for anionic clusters.

Our observation of primarily small cobalt oxide anion products containing one or two cobalt atoms differs from the observation of products for cobalt cluster cations. Castleman and co-workers[20] found that the major product channel in the size range $n = 3-9$ is addition accompanied by loss of a neutral atom ($Co_n^+ + O_2 \rightarrow Co_{n-1}O_2^+ + Co$). Freas et al.[61] investigated reactions of cobalt cluster cations with O_2 in a chemical ionization/fast atom bombardment (CI/FAB) source. They found three different ion product pathways: oxygen deficient products $(Co(CoO)_x)^+$, oxygen equivalent products $((CoO)_x)^+$, and to a much lesser extent metal deficient products $((CoO)_xO)^+$. Freas et al. attribute this behavior to the electropositivity of the cobalt atom, which can accommodate the positive charge. When this idea is extended to our anionic

systems, the negative charge would be expected to stay with the oxygen-rich, cobalt-poor smaller fragments, leaving the larger cobalt cluster fragment neutral, as generally observed. The major product is CoO_2^-, and other intermediate products are also relatively oxygen−rich anions. Negative charge appears to promote "etching" type reaction via formation of a small cobalt oxide anion like CoO_2^-, while positive charge tends to promote loss of neutral cobalt atoms with adsorption (presumably dissociative) of oxygen on the larger, positive cluster fragment.

4.3. Carbon Monoxide. On cobalt and other transition metal surfaces, CO generally adsorbs perpendicular to the surface by bonding through the carbon atom.[62−64] Both atom on-top and bridging adsorption sites are observed for CO on cobalt, with binding energies[56−58] of 100−145 kJ/mol. Local density theory calculations yield binding energies of 118 kJ/mol for 3-fold face sites, 135 kJ/mol for 2-fold bridging sites, and 154 kJ/mol for on-top sites.[58] In organometallic complexes, CO ligands likewise bind to transition metals in terminal, 2-fold bridging, and 3-fold face sites. In many transition metal carbonyls, including for example $Co_4(CO)_{12}$, the ligands are "fluxional" in solution, undergoing exchange between sites on the NMR time scale.[45,65,66] Carbonyl ligands and adsorbates bind by both σ donation from the carbon lone pair to empty metal orbitals and by π-back-bonding from the metal to the unoccupied antibonding orbital on CO.[59,67]

4.3.1. Addition versus Fragmentation. The rapid addition of CO molecules to cobalt clusters is indicative of the strong cobalt−carbonyl interaction and formation of covalently chemisorbed carbonyls. Fragmentation (loss of Co atoms upon CO addition) is also a substantial reaction pathway. That implies that the CO binding energies to the clusters are greater than the cobalt−cobalt bond energies, 1.5−3.5 eV depending on size (Figure 8), particularly for the initial additions. The larger clusters produced greater fragmentation versus addition products, compared with smaller clusters. That is opposite what we might expect from unimolecular dissociation rate theory−since fragmentation channels compete with stabilization of addition products by buffer gas collisions, the nascent complexes for larger clusters should be more easily stabilized than small clusters because of longer lifetimes due to their higher metal−metal binding energies (Figure 8) and their larger numbers of degrees of freedom. Evidently, the buffer gas collisions cannot drain energy fast enough to prevent fragmentation in the case of rapid multiple additions of carbonyls. The larger clusters bind more carbonyls than the smaller clusters, and each additional CO ligand adds energy to the cluster.

4.3.2. Cluster Charge Effects. Morse et al.[6] and Cox et al.[13] studied the reactivity of neutral cobalt clusters with CO. The relative reaction rates increase with cluster size[6] with little size-selectivity, similar to our results for anions (Figure 3). Addition of CO ligands was observed,[13] with Co_n adding one carbonyl for clusters for $n = 2-4$ and two carbonyls for $n = 5-14$. Under the experimental conditions for the neutral cluster studies,[13] saturation limits are not detected. In the present experiments, saturation limits for $n \leq 6$ can be observed because of longer experimental reaction times and because of faster collision rates and longer lifetimes of the nascent complexes (which promotes collisional stabilization) due to the strong charge/induced-dipole interactions for ionic clusters. Castleman and co-workers[14] investigated cobalt cluster cations ($n = 2-8$) in their SIDT-LV apparatus. Similar to the anions, they found that carbonyls adsorbed sequentially onto the cationic cobalt clusters up to size-dependent saturation limits. The reaction rate coefficients increase with size, reaching the collision rate by $n = 4$, following the same general behavior for neutrals and anions, although the reaction efficiencies are higher than what we observe. The Co_6^+ cluster reacts more slowly than its neighbors,[14] which is an exceptional case of size-selective reactivity with CO not seen for neutrals or anions.

4.3.3. Saturation Limits. The saturation limits (Table 2) can crudely be considered in terms of coverage, defined as the ratio of the number of carbonyls to the number of cobalt atoms. Maximum coverages range from 3.3 for the Co_3^- cluster to 2.3 for the Co_7^- cluster. One would expect coverages on the order of unity or less in the limit of a bulk cobalt surface, but small clusters can ligate more than one carbonyl per atom.[68] On small clusters, steric effects are not the primary limitation on the number of carbonyls. Rather, the number of molecular orbitals available for electron donation, after accounting for those used in metal−metal bonding, controls the number of ligands. That concept is the basis for electron-counting rules in organometallic chemistry, which have been very successful in correlating the skeletal structures of metal cluster compounds with the number of cluster valence electrons (CVEs) from the metal atoms and ligands.[44−50] These ideas have previously been applied to gas-phase metal clusters.[14,21,22,51−54] We use polyhedron skeletal electron pair theory (PSEPT)[46] applied to clusters as described previously[53,54] to predict skeletal structures for the saturated species. Castleman and co-workers[14] have similarly used these arguments for cationic $Co_n(CO)_m^+$ species. We cannot definitely assign the structures with respect to positions of the carbonyls but may speculate based on known condensed-phase analogues.

Carbonyl saturation limits, CVE counts, and predicted structures from PSEPT for the saturated species are summarized in Table 2 for $Co_n(CO)_m^-$ from this work and for $Co_n(CO)_m^+$ from Castleman and co-workers.[14] We also list the intermediate stable species or "magic numbers" [14] from both studies. Figure 8 of our previous work on platinum cluster carbonyls[53] shows predicted CVE counts for a variety of structures of small clusters from which the structures in Table 2 may conveniently be taken.

Dimer. The dicobalt species ligates a maximum of seven carbonyls, corresponding to 33 CVEs (nine electrons for each sd^8 cobalt atom, two for each carbonyl, plus one for the excess charge), although $m = 6$ is also stable. $Co_2(CO)_7^-$ is isoelectronic with the saturated cation $Co_2(CO)_8^+$,[14] both of which have one fewer electron than the observed neutral dicobalt carbonyl,[65,66,69] $Co_2(CO)_8$ with 34 CVEs. The addition of another carbonyl to the ionic gas-phase species would add two CVEs, one beyond the closed shell (the even n ionic clusters have an odd number of electrons). $Co_2(CO)_8$ has two major isomeric forms,[66] one with all-terminal carbonyls and the other with six terminal and two bridging carbonyls. It is possible that the undercoordinated species $Co_2(CO)_6^-$ is relatively stable because of an activation energy for changing geometry to accommodate another ligand−for example, if the seventh carbonyl is the first to occupy a bridging site.

Trimer. The tricobalt anion saturates with 10 carbonyls, corresponding to 48 CVEs. According to PSEPT rules, that number is typical for a triangular metal trimer. The binding sites of the carbonyls cannot be predicted by PSEPT, although one could imagine three carbonyls per cobalt atom in equatorial terminal and/or 2-fold bridging sites, with the 10th carbonyl in a 3-fold face site. For the tricobalt cation,[14] the saturated species was $Co_3(CO)_{10}^+$, which has only 46 CVEs compared with 48 expected for a triangular core and 50 expected for the linear form. The authors attributed this to an "imperfect triangular structure".[14] A reduction of metal−metal bonding from three two-electron bonds of the triangular species should *increase* the

number of carbonyls that can ligate, not decrease it. Therefore, multiple metal−metal bonds or steric effects must be invoked to explain $Co_3(CO)_{10}^+$. The intermediate stable anion observed here, $Co_3(CO)_8^-$, has too few ligands to be coordinatively saturated. It is suggestive of a symmetric species where each of the three terminal, three 2-fold bridging, and two 3-fold face sites of a triangular species are singly ligated. Addition of carbonyls beyond eight might force the ligands into less favorable binding orientations.

Tetramer. The tetracobalt anion has a saturation limit of 12 CO ligands or 61 CVEs, which best corresponds with a butterfly structure (square or rhombus with an extra metal−metal bond between two atoms on opposite corners). However, the species with 11 carbonyls (59 CVEs), which would be expected to have a tetrahedral cobalt framework (60 CVEs predicted by PSEPT), is most abundant up to the highest accessible CO concentrations. The tetracobalt cation[14] saturates with 12 CO ligands, also with 59 CVEs, and assigned as tetrahedral. The condensed-phase neutral compound $Co_4(CO)_{12}$ is described as having a tetrahedral core with an icosahedral cage of carbonyls, fluxional above 52 °C for the solid and 30 °C for the liquid.[45,69] For low-temperature crystals,[70] the assigned structure has an apical $Co(CO)_3$ group and three basal $Co(CO)_2$ groups plus three edge-bridging carbonyls around the base (total of nine terminal and three bridged carbonyls). Since $Co_4(CO)_{11}^-$ is a stable intermediate and its electron counts agree with a tetrahedral structure along with $Co_4(CO)_{12}^+$ and $Co_4(CO)_{12}$, it seems likely that the tetrahedron is initially formed.

The slow addition of the 12th carbonyl to form $Co_4(CO)_{12}^-$ might correspond to a change in geometry with an activation barrier, e.g., breaking a metal−metal bond in the tetrahedron to isomerize to a butterfly skeleton. An intriguing alternative would be maintaining the tetrahedral structure with a negatively charged metal cluster core surrounded by an icosahedral cage of 12 carbonyls, as in the fluxional neutral compound. For the cation, 12 carbonyls already satisfy the CVE counts for a tetrahedron, so no similar transition would be required.

Pentamer. The saturated pentamer cluster anion with 13 carbonyls has 72 CVEs, which is the correct number for a trigonal bipyramid metal skeleton. The pentamer cation[14] has a maximum coordination number of 14 CO ligands, also giving 72 CVEs, and is assigned as a trigonal bipyramid. This behavior implies that the number of electrons, not the number of ligands, is the overriding factor for the saturation limit for the pentamer. Intermediate stable species are observed with nine carbonyls for the anion and with eight and nine carbonyls for the cation. These are too few ligands to satisfy all of the molecular orbitals, except by multiple metal−metal bonding. A trigonal bipyramid has nine edges, which is suggestive of bridging carbonyls forming first with geometric factors (binding site differences or ligand−ligand interactions) making further CO addition less facile.

Hexamer. The hexacobalt anion has a saturation limit of 15 ligands for a total of 85 CVEs. Castleman and co-workers[14] also observed 85 CVEs for the saturated cationic hexamer, with 16 carbonyls, and assigned it as an octahedral structure. Although an octahedron is attractive because of its inherent symmetry, three other structures are predicted by PSEPT to have the same CVE counts, namely, a monocapped square pyramid, a bridged trigonal bipyramid, and edge-fused tetrahedrons. Thus, the structures of the gas-phase hexacobalt carbonyl ions cannot be uniquely assigned based solely on their electron counts. Condensed-phase studies[65,71−73] have examined hexacobalt carbonyls, including $Co_6(CO)_{16}$, $Co_6(CO)_{15}^{2-}$, and $Co_6(CO)_{14}^{4-}$, all three of which have confirmed octahedral structures. In analogy to the condensed-phase species, it thus seems reasonable that the gas-phase hexacobalt carbonyl ions are indeed octahedral. The placement of the carbonyls varies with charge state for the condensed-phase compounds. As the negative charge increases, there is an increase in the number of bridged carbonyls and a decrease in the number of terminally bound carbonyls, which is attributed to a greater electron-withdrawing effect for bridged carbonyls.[71,73] One might guess, therefore, that the gas-phase anion and cation species could have different arrangements of carbonyls with respect to binding sites (among many possibilities for 15−16 ligands on an octahedron), while the number of carbonyls is controlled by satisfying the cluster valence electron counts.

Both the anion and cation hexacobalt species exhibit intermediate stable species with 12 CO ligands. As with the pentamer, that suggests the intermediate kinetic bottlenecks result from geometric factors. An octahedron has 12 edges, which further suggests rapid addition to 2-fold bridge sites followed by slower addition to terminal or face positions.

Heptamer. The heptamer anion was observed to add at least 16 CO ligands for a total of 96 CVEs, which corresponds to either a tricapped tetrahedron or a bicapped trigonal bipyramid in PSEPT (both also can be described as face-fused tetrehedrons). However, full saturation is probably not achieved in this case (see section 3.2). Castleman and co-workers[14] observed a saturation limit of 19 carbonyls (100 CVEs) for the heptacobalt cation, which they assigned as a pentagonal bipyramid. If the present limit of 16 carbonyls is actually an intermediate stable species rather than the true limit for electronic saturation, in analogy to the pentamer and hexamer one might predict a structure with 16 edges. That does *not* correspond to a pentagonal bipyramid, however, which has 15 edges. For the cation, an intermediate stable species was found with the addition of 14 CO ligands, which is also different from the anions. Thus, although the cations and anions of the pentamer and hexamer show similar behavior in terms of electronic and geometric ligation limits, no consistent picture emerges for the heptamer. Furthermore, the increasing number of possible structures with increasing size makes application of electron-counting rules ambiguous for heptamer and larger species.

4.3.4. Comparison with Structures of Bare Clusters. The structures derived using PSEPT apply strictly only to the carbonylated species but may be compared with bare clusters in the limit that ligation does not cause geometry changes. Density functional calculations[43] predict triangular and tetrahedral structures for Co_3 and Co_4, respectively, which are consistent with the skeletal structures found for the anionic and cationic carbonyls (Table 2). The tetramer anion may change geometry from tetrahedral to butterfly upon the slow addition of its 12th carbonyl. In recent work, Riley and co-workers[17] have used adsorption of N_2 as a chemical probe of structures for neutral cobalt clusters. They also found a triangular structure for the trimer and assigned a tetrahedral structure for the tetramer that may open up to a square or butterfly upon further addition of nitrogen. Riley and co-workers propose a trigonal bipyramid for the pentamer cluster and an octahedron for the hexamer, also consistent with the ionic carbonyls (Table 2). The relatively high dissociation energies of the bare hexamers (Figure 8) for cations, neutrals, and anions are also consistent with octahedral structures, as previously suggested[34] for Co_6^+. Although these structural assignments are all based on indirect evidence, the consistency of various experiments suggests that the bare and carbonylated clusters generally have the same geometries. The

geometries point to near-maximum metal−metal bonding for the bare cobalt clusters.

4.4. Nitrogen. In stark contrast with the observed extreme lack of reactivity of the small cobalt cluster anions with nitrogen, neutral[6,16,17] and cationic[12,15] cobalt clusters react with N_2 at easily observable rates. Those reactions show strong size-selectivity, i.e., large differences in rates for various cluster sizes.[12,15] Riley and co-workers[17] observe multiple additions of N_2 to small neutral cobalt clusters and also report intermediate plateaus in the nitrogen uptake plots that they interpret as changes in cluster geometry. They characterize the bonding as molecular with one nitrogen molecule per surface metal atom. These observations indicate that nitrogen is very much more reactive with cationic and neutral cobalt clusters than what we observe for the anions. Smalley and co-workers[15] observed that cationic cobalt clusters reacted faster with CO than neutral clusters. Thus, the trend in cobalt cluster reactivity appears to follow the order cations > neutrals > anions, which suggests that addition is promoted by transfer of electron density from nitrogen to the metal. We do observe extremely slow addition of N_2 to the largest cluster anions studied, Co_7^- and Co_8^-. That might be rationalized by the delocalization of the negative charge such that the larger cluster anions are not as electronegative. The larger number of degrees of freedom for the larger clusters may also promote collisional stabilization of weakly adsorbed nitrogen adducts.

5. Conclusion

The reactions of cobalt cluster anions with O_2, CO, and N_2 gases show enormous differences, both in reaction efficiencies and product formation channels. Oxygen reacts rapidly via "etching" type processes to form CoO_2^- and other oxygen-rich oxide anions, in contrast with the reactions of cobalt cluster cations[18−20] that yield cobalt-rich oxide cations. Nitrogen is largely inert with the small cobalt cluster anions, very slowing adding a single nitrogen molecule only to the largest sizes studied ($n = 7-8$), in dramatic contrast with neutral[6,15−17] and cationic[12,15] cobalt clusters for which nitrogen addition is readily observed.

Carbon monoxide reacts by multiple sequential addition up to saturation limits that can be correlated with skeletal structures based on electron-counting rules. The anionic and previously studied cationic[14] carbonyl-saturated cobalt clusters have different numbers of carbonyls but the same number of cluster valence electrons for $n = 2$, 5, and 6, implying that they possess identical skeletal structures as determined by electronic molecular orbital considerations. For $n = 3$ and 4 clusters, however, the anionic and cationic species saturate with the same number of carbonyls (but different electron counts), suggesting that geometric factors (binding site effects or ligand−ligand interactions) can also be important. For $n = 5$ and $n = 6$, intermediate stable species with the same number of carbonyls (9 and 12, respectively) for the anions and cations suggest kinetic stability due to geometric factors, perhaps with all 2-fold bridging carbonyls for the proposed skeletal structures (trigonal bipyramid and octahedron, respectively). These intermediate species then react more slowly to saturation limits that can be explained by electron-counting rules. Theoretical calculations on cobalt cluster carbonyls and measurements of the metal−carbonyl binding energies would be useful in providing definitive structural assignments.

Acknowledgment. This research has been sponsored by the National Science Foundation under Grant CHE-9423326. Acknowledgment is also made to the donors of the Petroleum Research Fund, administered by the American Chemical Society, for partial support of this research.

References and Notes

(1) Parent, D. C.; Anderson, S. L. *Chem. Rev. (Washington, D.C.)* **1992**, *92*, 1541−1565.
(2) Riley, S. J. In *Clusters of Atoms and Molecules II*; Haberland, H., Eds.; Springer: Berlin, 1994; pp 221−240.
(3) Geerlings, J.; Zonnevylle, M. C.; de Groot, C. P. M. *Surf. Sci.* **1991**, *241*, 302−314.
(4) Geerlings, J.; Zonnevylle, M. C.; de Groot, C. *Surf. Sci.* **1991**, *241*, 315−324.
(5) Geusic, M. E.; Morse, M. D.; Smalley, R. E. *J. Chem. Phys.* **1985**, *82*, 590−591.
(6) Morse, M. D.; Geusic, M. E.; Heath, J. R.; Smalley, R. E. *J. Chem. Phys.* **1985**, *83*, 2293−2304.
(7) Kaldor, A.; Cox, D. M. *J. Chem. Soc., Faraday Trans.* **1990**, *86*, 2459−2463.
(8) Ho, J.; Zhu, L.; Parks, E. K.; Riley, S. J. *J. Chem. Phys.* **1993**, *99*, 140−147.
(9) Ho, J.; Zhu, L.; Parks, E. K.; Riley, S. J. *Z. Phys. D.* **1993**, *26*, 331−333.
(10) Parks, E. K.; Nieman, G. C.; Riley, S. J. *Surf. Sci.* **1996**, *355*, 127−139.
(11) Andersson, M.; Persson, J. L.; Rósen, A. *J. Phys. Chem.* **1996**, *100*, 12222−12234.
(12) Nakajima, A.; Kishi, T.; Sone, Y.; Nonose, S.; Kaya, K. *Z. Phys. D.* **1991**, *19*, 385−387.
(13) Cox, D. M.; Reichmann, K. C.; Trevor, D. J.; Kaldor, A. *J. Chem. Phys.* **1988**, *88*, 111−119.
(14) Guo, B. C.; Kerns, K. P.; Castleman, A. W., Jr. *J. Chem. Phys.* **1992**, *96*, 8177−8186.
(15) Brucat, P. J.; Pettiette, C. L.; Zheng, L.-S.; Craycraft, M. J.; Smalley, R. E. *J. Chem. Phys.* **1986**, *85*, 4747−4748.
(16) Parks, E. K.; Zhu, L.; Ho, J.; Riley, S. J. *Z. Phys. D* **1993**, *26*, 41−45.
(17) Ho, J.; Parks, E. K.; Zhu, L.; Riley, S. J. *Chem. Phys.* **1995**, *201*, 245−261.
(18) Jacobson, D. B.; Freiser, B. S. *J. Am. Chem. Soc.* **1986**, *108*, 27−30.
(19) Hales, D. A.; Armentrout, P. B. *J. Cluster Sci.* **1990**, *1*, 127−142.
(20) Guo, B. C.; Kerns, K. P.; Castleman, A. W., Jr. *J. Phys. Chem.* **1992**, *96*, 6931−6937.
(21) Pan, Y. H.; Sohlberg, K.; Ridge, D. P. *J. Am. Chem. Soc.* **1991**, *113*, 2406−2411.
(22) Ridge, D. P. In *Unimolecular and bimolecular ion-molecule reaction dynamics*; Ng, C. Y., Baer, T., Powis, I., Eds.; John Wiley & Sons: Chichester, 1994; pp 337−370.
(23) Irion, M. P.; Schnabel, P.; Selinger, A. *Ber. Bunseges. Phys. Chem.* **1990**, *94*, 1291−1295.
(24) Irion, M. P. *Int. J. Mass Spectrom. Ion Processes* **1992**, *121*, 1−47.
(25) Nonose, S.; Sone, Y.; Kikuchi, N.; Fuke, K.; Kaya, K. *Chem. Phys. Lett.* **1989**, *158*, 152−156.
(26) Klots, T. D.; Winter, B. J.; Parks, E. K.; Riley, S. J. *J. Chem. Phys.* **1990**, *92*, 2110−2111.
(27) Klots, T. D.; Winter, B. J.; Parks, E. K.; Riley, S. J. *J. Chem. Phys.* **1991**, *95*, 8919−8930.
(28) Winter, B. J.; Klots, T. D.; Parks, E. K.; Riley, S. J. *Z. Phys. D.* **1991**, *19*, 375−380.
(29) Winter, B. J.; Klots, T. D.; Parks, E. K.; Riley, S. J. *Z. Phys. D.* **1991**, *19*, 381−394.
(30) Parks, E. K.; Winter, B. J.; Klots, T. D.; Riley, S. J. *J. Chem. Phys.* **1992**, *96*, 8267−8274.
(31) Riley, S. J. *Ber. Bunsen-Ges. Phys. Chem.* **1992**, *96*, 1104−1109.
(32) Parks, E. K.; Klots, T. D.; Winter, B. J.; Riley, S. J. *J. Chem. Phys.* **1993**, *99*, 5831−5839.
(33) Pellarin, M.; Baguenard, B.; Vialle, J. L.; Lermé, J.; Broyer, M.; Miller, J.; Perez, A. *Chem. Phys. Lett.* **1994**, *217*, 349−356.
(34) Hales, D. A.; Su, C.-X.; Lian, L.; Armentrout, P. B. *J. Chem. Phys.* **1994**, *100*, 1049−1057.
(35) Russon, L. M.; Heidecke, S. A.; Birke, M. K.; Conceicao, J.; Armentrout, P. B.; Morse, M. D. *Chem. Phys. Lett.* **1993**, *204*, 235−240.
(36) Russon, L. M.; Heidecke, S. A.; Birke, M. K.; Conceicao, J.; Morse, M. D.; Armentrout, P. B. *J. Chem. Phys.* **1994**, *100*, 4747−4755.
(37) Parks, E. K.; Klots, T. D.; Riley, S. J. *J. Chem. Phys.* **1990**, *92*, 3813−3826.
(38) Yang, S.; Knickelbein, M. B. *J. Chem. Phys.* **1990**, *93*, 1533−1539.
(39) Minemoto, S.; Terasaki, A.; Kondow, T. *J. Chem. Phys.* **1996**, *104*, 5770−5775.
(40) Leopold, D. G.; Lineberger, W. C. *J. Chem. Phys.* **1986**, *85*, 51−55.

(41) Yoshida, H.; Terasaki, A.; Kobayashi, K.; Tsukada, M.; Kondow, T. *J. Chem. Phys.* **1995**, *102*, 5960−5965.
(42) Li, Z.-Q.; Gu, B.-L. *Phys. Rev. B* **1993**, *47*, 13611−13614.
(43) Jamorski, C.; Martinez, A.; Castro, M.; Salahub, D. R. *Phys. Rev. B* **1997**, *55*, 10905−10921.
(44) Lauher, J. W. *J. Am. Chem. Soc.* **1978**, *100*, 5305−5314.
(45) Khara, K. C.; Dahl, L. F. *Adv. Chem. Phys.* **1988**, *70* (Part II), 1−43.
(46) Owen, S. M. *Polyhedron* **1988**, *7*, 253−283.
(47) Mingos, D.; Slee, T.; Zhengyang, L. *Chem. Rev. (Washington, D.C.)* **1990**, *90*, 383−402.
(48) Teo, B. K. *Inorg. Chem.* **1984**, *23*, 1251−1257.
(49) Teo, B. K.; Longoni, G.; Chung, F. R. K. *Inorg. Chem.* **1984**, *23*, 1257−1266.
(50) Teo, B. K. *Inorg. Chem.* **1985**, *24*, 4209−4213.
(51) Fayet, P.; McGlinchey, M. J.; Wöste, L. *J. Am. Chem. Soc.* **1987**, *109*, 1733−1738.
(52) Mingos, D. P.; Wales, D. J. *J. Am. Chem. Soc.* **1990**, *112*, 930−932.
(53) Ren, X.; Hintz, P. A.; Ervin, K. M. *J. Chem. Phys.* **1993**, *99*, 3575−3587.
(54) Hintz, P. A.; Ervin, K. M. *J. Chem. Phys.* **1994**, *100*, 5715−5725.
(55) Rao, C.; Kamath, P. V.; Yashanath, S. *Chem. Phys. Lett.* **1982**, *88*, 13−16.
(56) Benziger, J. B. *Appl. Surf. Sci.* **1980**, *6*, 105−121.
(57) Papp, H. *Ber. Bunsen-Ges. Phys. Chem.* **1982**, *86*, 555−562.
(58) Zonnevylle, M. C.; Geerlings, J. J. C.; van Santen, R. A. *J. Catal.* **1994**, *148*, 417−426.
(59) Brodén, G.; Rhodin, T. N.; Brucker, C.; Benbow, R.; Hurych, Z. *Surf. Sci.* **1976**, *59*, 593−611.
(60) Somorjai, G. A. *Chemistry in Two Dimensions: Surfaces*; Cornell University Press: Ithaca, NY, 1981.
(61) Freas, R. B.; Dunlap, B. I.; Waite, B. A.; Campana, J. E. *J. Chem. Phys.* **1987**, *86*, 1276−1288.
(62) Rao, C.; Rao, G. R. *Surf. Sci. Rep.* **1991**, *13*, 221−263.
(63) Horn, K.; DiNardo, J.; Eberhardt, W.; Freund, H.-J.; Plummer, E. W. *Surf. Sci.* **1982**, *118*, 465−495.
(64) Greuter, F.; Heskett, D.; Plummer, E. W.; Freund, H.-J. *Phys. Rev. B* **1983**, *27*, 7117−7133.
(65) Kemmitt, R. D. W.; Russell, D. R. In *Comprehensive Organometallic Chemistry*; Wilkinson, G., Stone, F. G. A., Abel, E. W., Eds.; Pergamon: Oxford, 1982; Vol. 5, pp 1−276.
(66) Onaka, S.; Shriver, D. F. *Inorg. Chem.* **1976**, *15*, 915−918.
(67) Blyholder, G. *J. Phys. Chem.* **1964**, *68*, 2772−2778.
(68) Falo, F.; Cano, I.; Salmerón, M. *Surf. Sci.* **1984**, *143*, 303−131.
(69) Hanson, B. E.; Lisic, E. C. *Inorg. Chem.* **1986**, *25*, 715−716.
(70) Wei, C. H.; Dahl, L. F. *J. Am. Chem. Soc.* **1966**, *88*, 1821−1822.
(71) Albano, V.; Chini, P.; Scatturin, V. *J. Organomet. Chem.* **1968**, *15*, 423−432.
(72) Mingos, D. *J. Chem. Soc., Dalton Trans.* **1974**, 133−138.
(73) Albano, V. G.; Bellon, P. L.; Chini, P.; Scatturin, V. *J. Organomet. Chem.* **1969**, *16*, 461−470.